Experimental versus simulated Coulomb-explosion images of flexible molecules: Structure of protonated acetylene $C_2H_3^+$

Lars Knoll,[1] Zeev Vager,[2] and Dominik Marx[3]
[1]*Max-Planck-Institut für Kernphysik, Saupfercheckweg 1, 69029 Heidelberg, Germany*
[2]*Department of Particle Physics, Weizmann Institute of Science, Rehovot 76100, Israel*
[3]*Lehrstuhl für Theoretische Chemie, Ruhr-Universität Bochum, 44780 Bochum, Germany*
(Received 26 June 2002; published 28 February 2003)

The most probable structure of protonated acetylene $C_2H_3^+$ (the ''vinyl cation'') is inferred from both Coulomb-explosion experiments and finite-temperature *ab initio* quantum simulations followed by simulations of foil effects. It is found that $C_2H_3^+$ features significant deviations from the planar bridged equilibrium structure as well as from the planar Y-shaped local minimum structure, which are known from static electronic structure calculations. In particular, the ''axial protons'' feature a significant out-of-plane *trans*-bending due to fluctuation effects. This implies that the nonplanarity has to be taken into account in theoretical treatments that aim at describing this fluxional molecule.

DOI: 10.1103/PhysRevA.67.022506 PACS number(s): 33.15.−e, 31.15.Kb, 31.15.Ew

I. INTRODUCTION AND MOTIVATION

What is the ''structure'' of a molecule? There are different definitions of ''molecular structure'' as obtained either from experiment or from theory [1–3]. Among them is the ''equilibrium structure'' r_e that is determined from the minimum of the electronic ground-state potential-energy hypersurface. Although this structure is the one that is almost exclusively reported as a result of quantum-chemical geometry optimization calculations, it is not directly accessible in experiments. More realistic structural concepts are the ''average structure'' $\langle r \rangle$ (obtained from suitably averaging distance or position operators using the many-body nuclear wave function, most often in the quantum-mechanical rotational-vibrational ground state) or the ''most probable structure'' r_P (defined similarly, but based on the absolute maximum of the nuclear density) [3]. Spectroscopy, in particular infrared and microwave techniques, leads to the so-called ''r_0 structure.'' It is traditionally obtained by converting measured rotational constants into distances between nuclei that are assumed to behave like point particles. More sophisticated approaches rationalize the measured energy levels of a molecule in terms of a real-space structural model that best fits these spacings.

More recently, dramatic progress in determining more directly the real-space structure of molecules was made in the framework of Coulomb-explosion imaging (CEI) [4,5]. In CEI, the molecule's valence electrons get stripped off very rapidly when it passes in an accelerated beam through a thin target foil. This initiates an ''explosion'' of the molecular constituents, which is driven by internuclear Coulomb forces due to the lack of valence electrons and thus chemical bonding. The instantaneous molecular configuration at the moment of the stripping or explosion can be inferred from the velocities detected simultaneously using multiple-particle detectors, similar to more conventional scattering experiments. Such CEI experiments can yield information about the diagonal part of the fully correlated many-body nuclear density matrix of small molecules in real space. This implies that such experiments give access to both the average and the most probable structures, and even to the width of the distribution function along certain coordinates. As such, CEI experiments truly complement spectroscopy in that they offer a ''different view,'' i.e., real space versus Hilbert space, of the same molecule. However, a complication arises due to the fact that all primary information is given in ''velocity space'' (*V*-space). The so-called *V*-space to ''real-space'' (*R*-space) transformation has to take into account effects that occur during the explosion process within the target foil [6–10].

In the case of ''tame'' molecules, such as methane or acetylene, the different structural concepts lead to qualitatively and often also quantitatively similar answers. Using these two examples at hand, the situation changes radically once they become protonated to yield the CH_5^+ and $C_2H_3^+$ molecules. Both belong to the class of so-called ''flexible'' or ''fluxional'' molecules [11,12] that excert large-amplitude motion. Here, strongly anharmonic zero-point motion in conjunction with population of low-lying rovibrational states leads to significant excursions from the equilibrium structure. As a result, the average or most probable structures, might be quite different from the equilibrium structure and the theoretical ''normal mode'' or ''local mode'' concepts are of very limited use only. Thus, it is crucial to be able to have theoretical access to structures beyond the equilibrium structure.

In the case of $C_2H_3^+$, an ''important circumstellar and interstellar ion'' [13], electronic structure calculations unambiguously predict a planar equilibrium structure to be the global minimum on the potential-energy surface [14–21] if electron correlation is taken into account [14]. In this so-called ''bridged'' (or carbonium or nonclassical) structure, see Fig. 1(a), one proton forms a triangle with the two carbon nuclei, i.e., a three-center two-electron bond. The remaining two protons are essentially collinear with respect to the C—C bond axis. They are very slightly tilted *towards* the bridging proton, which was rationalized based on a topological analysis of the one-body electronic density [22]. The next higher-lying structure ($\approx$5 kcal/mol [19,21]) is the planar ''Y-shaped'' (or vinyl-cationic or classical) structure, see Fig.

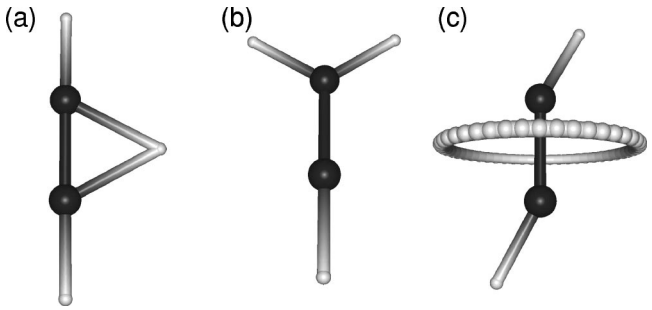

FIG. 1. Structures corresponding to the global minimum (a) and lowest local minimum (b) on the potential-energy surface of $C_2H_3^+$, which are denoted in the text as the ''bridged'' and ''Y-shaped'' structures, respectively. The sticks connecting the balls at the positions of the nuclei (C: large, black; H: small, gray) are included as guides to the eye and do not necessarily imply chemical bonds. The most probable structure according to CEI analysis and high-temperature simulations is shown in (c), see text for details. Note that this picture should only be considered as a sketch and not as a realistic representation in three-dimensional space.

1(b). To the best of our knowledge, previous theoretical treatments of possible dynamical rearrangements of this molecule were obtained by constraining all atoms to move in a common plane [23–27] with only two exceptions [28,29]. An interesting graph-theoretical analysis of nonrigid molecules including $C_2H_3^+$ is given in Ref. [30]. Based on infrared and millimeter spectroscopy [31–36,27], it is inferred that the bridged structure is favored. However, there is significant tunneling taking place so that some aspects of the spectra remain elusive. Pioneering CEI experiments on the $C_2H_3^+$ molecule [38,37] lead to a quite different structural proposal. In particular, a strongly nonplanar structure subject to dramatic large-amplitude motion, making $C_2H_3^+$ a highly fluxional molecule with strong deviations from the bridged equilibrium structure, was inferred from analyzing the five-dimensional CEI angular distribution function, see Fig. 1(c) for a very schematic representation and the related discussion in the text.

In the present study, the correlated *N*-body nuclear density of $C_2H_3^+$ as generated by quantum and classical Car-Parrinello finite-temperature simulation methods [39] is converted to the correponding *V*-space CEI distributions by simulating the effects of molecule-foil interactions. Thus, by going beyond a comparison of theoretical data in *R* space to experimental data in *V* space, this refines and extends previous experimental and theoretical works [37,29] considerably. This approach makes possible a most direct comparison of the CEI experimental data to theoretically simulated structures without any adjustable parameters.

II. METHODS

The simulations were carried out using the standard Car-Parrinello *ab initio* molecular-dynamics method [40] as well as its quantum extension, the so-called *ab initio* path integral method [41–44]. Both methods and the used CPMD program [45] are reviewed in detail in Ref. [39], so that we present here only the general idea. The basic idea for using these methods in the context of molecular physics [46] is to generate a canonical ensemble of configurations of the molecule by performing classical or path-integral molecular-dynamics simulations. The interactions that govern the dynamics and thus determine the most probable and average structures are obtained from concurrent electronic structure calculations; for more details on the calculations, we refer the reader to Ref. [29]. This allows treating complex molecules without constraining the dimensionality of the problem, i.e., without fixing the atoms to move in a common plane or keeping certain degrees of freedom, such as bond distance, fixed. In this paper, the word ''classical'' is used for those simulations where the nuclei are treated as point particles subject to classical mechanics. Hence in this approximation the nuclei are only subject to thermal fluctuations. The term ''quantum'' simulation is used if all nuclei are treated as quantum degrees of freedom within the path-integral approach to quantum mechanics. This implies that quantum-mechanical fluctuations, leading to phenomena such as zero-point motion and tunneling, are included in addition to the thermal effects. In both cases, *R*-space trajectories are obtained, which contain configurations that sample from the exact canonical (Boltzmann) classical or quantum distribution function of the two carbon and three hydrogen nuclei $\tilde{\rho}(\mathbf{R}_{C^{(1)}},\mathbf{R}_{C^{(2)}},\mathbf{R}_{H^{(1)}},\mathbf{R}_{H^{(2)}},\mathbf{R}_{H^{(3)}})$ in Cartesian space. Thus, these configurations can be used to compute approximately, by averaging, the many-body nuclear density distribution function $\rho(\mathbf{R}_{C^{(1)}},\mathbf{R}_{C^{(2)}},\mathbf{R}_{H^{(1)}},\mathbf{R}_{H^{(2)}},\mathbf{R}_{H^{(3)}})$ in *R* space, which is the diagonal part of the many-body nuclear density matrix; note that this is a nine-dimensional function in terms of non-redundant *internal* coordinates.

In addition, the CEI process was subsequently simulated based on these trajectories using established methods [6–10]. However, up to the present investigation, these techniques were only used in conjunction with molecular *models*. In a nutshell, for each molecular configuration in *R*-space $(\mathbf{R}_{C^{(1)}},\mathbf{R}_{C^{(2)}},\mathbf{R}_{H^{(1)}},\mathbf{R}_{H^{(2)}},\mathbf{R}_{H^{(3)}})$, the Coulomb-explosion process is mimicked by chopping it up into small propagation periods interrupted by scattering and charge-exchange events. The scattering and charge-exchange processes in the target foil are simulated using a Monte Carlo procedure. In between these events the nuclei evolve subject to a suitably screened Coulomb interaction. After leaving the foil, the equations of motion of the nuclei are integrated further until the potential energy of the fragments has fallen below a given fraction of their initial energy. This yields the asymptotic velocities of the nuclei, from which the *V*-space coordinates of this particular initial configuration are directly obtained. The final distribution is obtained by averaging over the configurations sampled from the Car-Parrinello trajectories. This approach allows the comparison of experimental and theoretical distributions directly in *V* space without any adjustable parameter. This should be contrasted to concepts where the *R*-space distribution and thus most probable molecular structure is derived from *V*-space experimental data using inversion techniques [9]. The performance of this advanced analysis technique based on both path-integral simulations and experimental data was demonstrated in detail for small test systems, HD^+ and H_3^+, in Ref. [10].

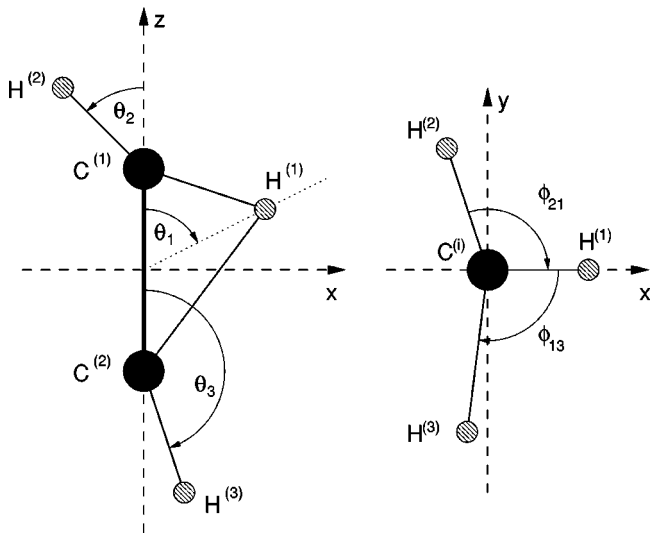

FIG. 2. Definition of the polar $(\theta_1,\theta_2,\theta_3)$ angles (left) and azimuthal (ϕ_{21},ϕ_{13}) angles (right), which are used to describe the angular arrangement of the protons within $C_2H_3^+$, and to define the permutational symmetry coordinates (E_1,E_2,S) according to Eq. (1). The $C^{(1)}$—$C^{(2)}$ bond defines the z axis, the atoms $(C^{(1)},H^{(1)},C^{(2)})$ span the x-z plane, and the y axis is perpendicular to that plane. The origin $(x,y,z)=(0,0,0)$ of this Cartesian coordinate system is at the C—C bond midpoint.

The structural analysis and comparison are performed in the most relevant internal coordinates of $C_2H_3^+$, which are the five angular coordinates for the three protons $i=1$, 2, 3 relative to the $z=$C—C bond axis as introduced in Ref. [37]. Specifically, these are two relative azimuthal angles (ϕ_{21},ϕ_{13}) between protons i and j around the z axis and three polar angles $(\theta_1,\theta_2,\theta_3)$, see Fig. 2 for the definition of all coordinates used. For convenience, the latter can be expressed [37] as permutational symmetry coordinates:

$$S=\sum_{i=1}^{3}\cos\theta_i$$

$$E_1=\frac{1}{\sqrt{6}}(2\cos\theta_1-\cos\theta_2-\cos\theta_3),$$

$$E_2=\frac{1}{\sqrt{2}}(\cos\theta_2-\cos\theta_3), \qquad (1)$$

so that the coordinate set $(E_1,E_2,\phi_{21},\phi_{13},S)$ defines unambiguously the angular arrangement of the three protons; note that S is a totally symmetric coordinate. In order to symmetrize the resulting distribution functions $\rho(E_1,E_2,\phi_{21},\phi_{13},S)$, the permutation symmetry is taken into account by permuting the proton labels explicitly. However, no smoothing of these distribution functions was applied, which is at variance to the previous analysis [37].

III. RESULTS AND DISCUSSION

The original experimental CEI data [37] were reanalyzed in V space in terms of the symmetry-adapted coordinates $(E_1,E_2,\phi_{21},\phi_{13},S)$ using the methods outlined in Sec. II, see Figs. 3(a–c) for an analysis of the corresponding distribution function $\rho(E_1,E_2,\phi_{21},\phi_{13},S)$ in terms of these coordinates. Note that no smoothing, such as the Gaussian broadening, used in the previous study [37] was applied in the present analysis. In the following, we explain our strategy in order to extract meaningful information from this high-dimensional distribution function that cannot be graphically represented without applying restrictions. The variation of the five-dimensional density distribution function $\rho(E_1,E_2,\phi_{21},\phi_{13},S)$ along the S coordinate (not shown) turn out to be unimodal, and features a prominent peak at $S=S^*=0$. Thus $S^*=0$ can be chosen as the most probable structural parameter along the S axis in order to simplify the subsequent configurational analysis. For this particular choice, $S^*=0$, the six degenerate maxima in the (E_1,E_2) plane of ρ are found to occur at about $(E_1\approx 0.0,E_2\approx 1.2)$ and five additional symmetry-equivalent points, see Fig. 3(a). According to the coordinate transformation (1), this symmetry-adapted configuration $(E_1\approx 0.0,E_2\approx 1.2,S^*=0)$ corresponds to $(\theta_1\approx 90°,\theta_2\approx 30°,\theta_3\approx 150°)$ in terms of the original polar angles defined in Fig. 2. Thus, according to this CEI experiment, configurations characterized by the polar angles $(\theta_1\approx 90°,\theta_2\approx 30°,\theta_3\approx 150°)$ contribute most significantly to the nuclear density matrix, and thus to the most probable structure—irrespective of the values of the two azimutal angles (ϕ_{21},ϕ_{13}). Note that this already implies a noncollinear arrangement of the four ''backbone'' atoms $H^{(2)}$—$C^{(1)}$—$C^{(2)}$—$H^{(3)}$. This already implies that the CEI-derived structure differs *qualitatively* from the bridged minimum-energy structure depicted in Fig. 1(a) since the latter would lead to $(\theta_1=90°,\theta_2=0°,\theta_3=180°)$ in the ideal collinear case and thus to $(E_1=0,E_2=0,S=0)$.

Having clarified the arrangement of the protons in the subspace spanned by the three polar angles, it remains to be analyzed how the protons are oriented with respect to each other in terms of their azimuthal angles. In order to be able to visualize such a high-dimensional distribution, we unfold the azimuthal subspace only for those *polar* angles that are most important according to the analysis in Fig. 3(a). Thus, we pick the maximum $(E_1^*,E_2^*)\approx(0.0,1.2)$ with $S^*=0$ as before and display the reduced distribution function of the remaining two coordinates (ϕ_{21},ϕ_{13}) only for the most important structure corresponding to $(E_1^*,E_2^*,S^*)\approx(0.0,1.2,0.0)$ or equivalently $(\theta_1\approx 90°,\theta_2\approx 30°,\theta_3\approx 150°)$. This procedure leads to two symmetry-equivalent maxima at about $(\phi_{21}\approx 110°,\phi_{13}\approx 110°)$ and $(\phi_{21}\approx 250°,\phi_{13}\approx 250°)$ in the azimuthal subspace, see Fig. 3(c). This implies that the three protons, and thus also the two carbon atoms, are not coplanar. Again, this is in contrast to both the bridged and Y-shaped structures shown in Figs. 1(a) and 1(b), respectively. The qualitative difference can be inferred from the definition of the azimuthal coordinates according to Fig. 2: the bridged and Y-shaped coplanar structures would lead to maxima at $(\phi_{21}=0°,\phi_{13}=0°)$ and $(\phi_{21}=0°,\phi_{13}\approx 180°)$,

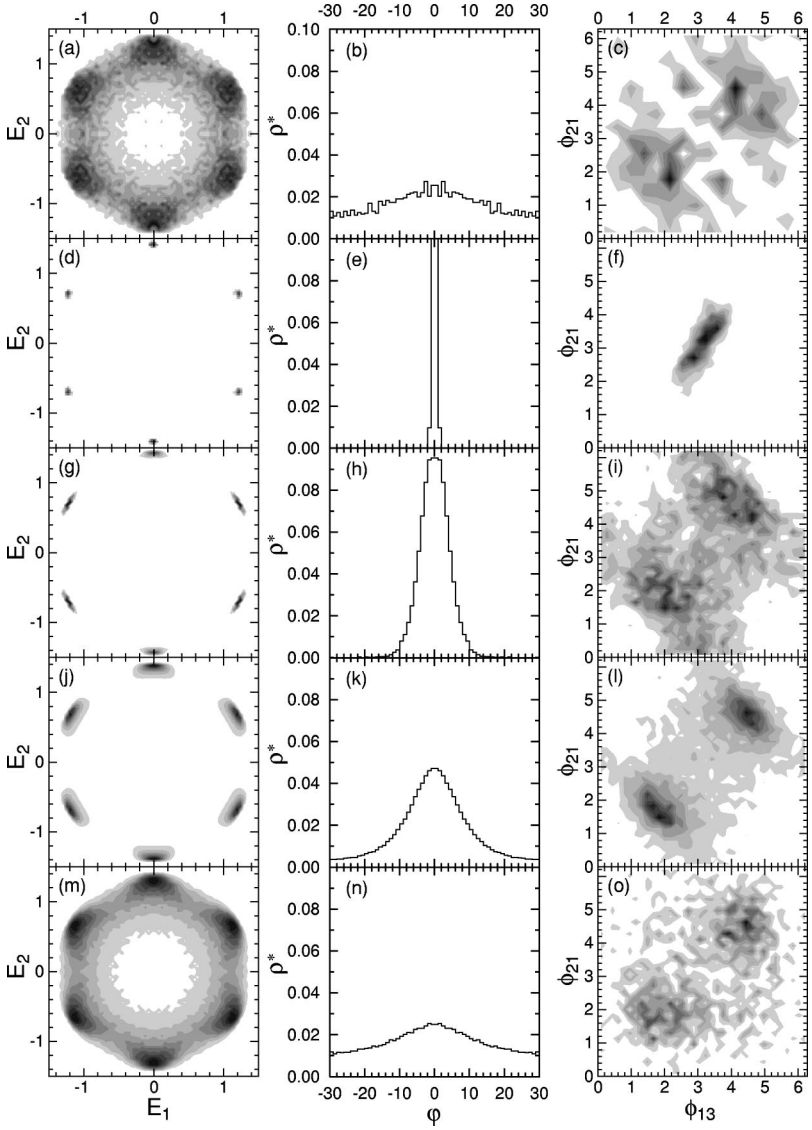

FIG. 3. Various partial representations of experimental and theoretical five-dimensional density distribution functions $\rho(E_1,E_2,\phi_{21},\phi_{13},S)$. Left column: projection onto (E_1,E_2) plane for fixed $S=S^*=0$; middle column: height variation in the (E_1,E_2) plane shown in the corresponding left column panel as parametrized by the polar angle $\varphi=\arctan(E_1/E_2)$; right column: unfolding of the distribution in the (ϕ_{21},ϕ_{13}) plane for fixed $(E_1,E_2)=(E_1^*,E_2^*)$ where E_1^* and E_2^* are defined by the (symmetry-equivalent) maxima in the (E_1,E_2) plane from the corresponding left column panel. Note that *each point* in the plane of the right column panels *exactly* defines one particular (angular) structure of $C_2H_3^+$ in terms of the symmetry-adapted coordinates $(E_1,E_2,\phi_{21},\phi_{13},S)$, and thus in terms of the angular coordinates $(\theta_1,\theta_2,\theta_3,\phi_{21},\phi_{13})$ as defined in Fig. 2. Panels (a)–(c): reanalyzed experimental *V*-space CEI distribution [37]; panels (d)–(f): simulated *R*-space CEI distribution at 5 K using classical nuclei; panels (g)–(i): simulated *R*-space CEI distribution at 5 K using quantum nuclei; panels (j)–(l): simulated *V*-space CEI distribution at 5 K using quantum nuclei; panels (m)–(o): simulated *V*-space CEI distribution at 3000 K using classical nuclei. In the contour plots, the density increases from white via gray to black, and the very narrow distribution (e) is shown only up to a value of $\rho^*=0.1$.

respectively, plus their symmetry-equivalent maxima.

Although there is certainly a preference for the noncollinear arrangement $(\theta_1\approx 90°,\theta_2\approx 30°,\theta_3\approx 150°)$ of the backbone atoms in view of the distribution presented in Fig. 3(a), there is also quite some density far away from these maxima. This stems from configurations that deviate from the most probable arrangement. The significance of such structures is quantified in Fig. 3(b) that shows the variation of the CEI distribution in the (E_1,E_2) plane from Fig. 3(a) as a function of the angle $\varphi=\arctan(E_1/E_2)$. The corresponding reduced density $\rho^*(\varphi)$ is periodic, and it is only shown for one segment between two minima; $\rho^*(\varphi)$ is shown for $S^*=0$ as in Fig. 3(a). The difference between the maximum and the minimum values of $\rho^*(\varphi)$ amounts to only about a factor of 2, which will be discussed in more detail at a later stage. This broadness in the subspace of the orientations of the protons relative to the *z* axis, i.e. $(\theta_1,\theta_2,\theta_3)$, is a feature of the pronounced nuclear motion of the protons relative to each other and relative to the C—C bond, see Fig. 2.

In summary, a first key feature of the most probable *V-space* structure derived from the CEI experiment is that the two ''axial protons'' are not collinear with respect to the C—C bond. They are tilted away from this axis by about $\theta_2\approx 30°$, and equivalently by about $\theta_3\approx 150°$. The third ''bridging proton,'' however, prefers to have an essentially perpendicular configuration $\theta_1\approx 90°$ with respect to the C—C bond axis. As a second key feature, the two axial protons and the two carbon atoms are not coplanar since $\phi_{ij}+\phi_{jk}\neq 0°$, 180°, or 360°. Pictorially, the two axial protons are arranged in a *trans*-bend orientation with respect to the plane spanned by the C—C bond and the briding proton. A very simplified sketch in real space, which is based on these experimental coordinates is presented in Fig. 1(c); we stress that this scheme should be considered as a caricature. This most probable structure derived from CEI experiments is *qualitatively* different from both the bridged and Y-shaped structures depicted in Figs. 1(a) and 1(b), respectively, and these differences are clearly detectable in the corresponding distribution functions in $(E_1,E_2,\phi_{21},\phi_{13},S)$ space. Finally, it is also clear that the molecule is subject to fluxionality or large-amplitude motion in view of its rather broad structural distribution functions.

The experimental CEI *V*-space patterns as unfolded in Fig. 3 are compared in Figs. 3(d)–3(f) to the corresponding ones obtained from classical *R*-space simulations at the very low temperature of 5 K. At such a low temperature the molecule is expected to be in its vibrational ground state. There is essentially no similarity between the experimental distribution and this classical low-temperature simulation—there are even crucial *qualitative* differences. In particular, the maxima in the unfolding of the three polar components of the distribution occur at $(E_1 \approx 0, E_2 \approx 1.41, S=0)$ and the five other permutation symmetry-equivalent locations. This is very close to $(E_1=0, E_2=\sqrt{2}, S=0)$, or equivalently $(\theta_1=90°, \theta_2=0°, \theta_3=180°)$, which defines a collinear $H^{(2)}$—C—C—$H^{(3)}$ arrangement of the C—C bond axis and the two axial protons, while the bridging proton $H^{(1)}$ is perpendicular with respect to the *z* axis, see Fig. 2 and Eq. (1). Thus, the corresponding *R*-space structure is essentially the one of the global minimum of the potential-energy surface, which is the bridged structure in Fig. 1(a). It is characterized by an essentially linear $H^{(2)}$—C—C—$H^{(3)}$ backbone where the third proton $H^{(1)}$ is attached rigidly in a bridging position with respect to both carbon atoms. Permuting the $H^{(i)}$'s labels and thus the protons yields the six symmetry-equivalent structures that lead to the six degenerate maxima in Fig. 3(d). Furthermore, the peaks of the distribution in the $(E_1, E_2, S^*=0)$ plane are slightly broadened δ-functions, and thus their width is much narrower than observed in experiment, see Figs. 3(d)–3(f). In particular, one can see in the one-dimensional cut in Fig. 3(e) that the polar angles feature a degree of localization that is essentially a δ-function; the corresponding distribution along the *S* coordinate (not shown) displays a similar sharp peak. This is very different from the corresponding experimental CEI *V*-space distribution $\rho^*(\varphi)$ from Fig. 3(b).

Since the protons are light particles, the next logical step consists of including nuclear quantum effects, which is done here by treating *all* nuclei as quantum degrees of freedom at the same temperature of 5 K. At a first glance the agreement with experiment does not seem to improve much: the (E_1, E_2) distribution for $S^*=0$ is again very narrow, see Fig. 3(g). However, one can observe significant broadening effects in this *R*-space distribution due to quantum-mechanical fluctuations: the cut in Fig. 3(h) is no longer a δ-function akin to the one in Fig. 3(e). In addition, a closer analysis reveals that the maximum is slightly shifted away from the ideal collinear orientation $(E_1=0, E_2=\sqrt{2}, S=0)$ to a value of $(E_1 \approx 0, E_2 \lesssim \sqrt{2}, S=0)$; note that this difference can be hardly seen from the graphical representation of the numerical data. This signals a small but significant deviation of the two axial protons $H^{(2)}$ and $H^{(3)}$ from being collinear with respect to the C—C axis, i.e. $(\theta_1 \approx 90°, \theta_2 \gtrsim 0°, \theta_3 \lesssim 180°)$, see Fig. 2. Most importantly, the defolding in the remaining (ϕ_{21}, ϕ_{13}) plane is *qualitatively* consistent with the experimental *V*-space data. A direct comparison of Fig. 3(i) to Fig. 3(c) shows that the maxima are close to those found experimentally. Thus, the three protons and the two carbon atoms are clearly no longer coplanar as in the classical simulation at the same temperature, which must be an effect of the quantum fluctuations that are included in Figs. 3(g)–3(i), but not in Figs. 3(d)–3(f). Still, the magnitude of the *trans*-bending of the axial protons with respect to the C—C axis is much less pronounced than experimentally observed. Thus, the comparison is far from being satisfactory and conclusive. First of all, the deviations from collinearity amount to only a few degrees at most. Furthermore, although the quantum distribution along the circular cut through the $(E_1, E_2, S=0)$ distribution, as parameterized by the φ coordinate in Fig. 3(h), is considerably broader than the corresponding classical one in Fig. 3(e), this does not feature a significant density at the *minima* around $\varphi \approx \pm 30°$. Note, in particular, that the height of the minima of the experimental distribution in Fig. 3(b) is about 1/2 of that of the maxima, whereas in the quantum simulation the value at the minima is zero. Hence configurations that deviate very strongly from a collinear $H^{(2)}$—C—C—$H^{(3)}$ arrangement are very likely in the experiment, whereas they essentially do not occur in the quantum simulation at 5 K.

Up to this point, the comparison was done by computing the distribution function in *R*-space, whereas the experimental information is given in *V*-space. This is evidently an unsatisfactory approximation since it is expected that in general the *R*-space to *V*-space transformation folds in quite an amount of broadening into the distributions of bond angles or bond distances [5,47]. In order to allow for a truly quantitative comparison, it is mandatory to also include the foil artifacts in the simulations—in particular multiple-scattering and charge-exchange effects. Following the route outlined in Sec. II, exactly the same configurations that lead to the *R*-space distribution displayed in Figs. 3(g)–3(i) were used in order to generate the *R*-space to *V*-space transformation, see Figs. 3(j)–3(l). First of all, the simulated *V*-space distribution in the (E_1, E_2) plane broadens such that the minima aquire $\approx 8\%$ of the height of the maxima, see the φ-parametrized cut in Fig. 3(k). Interestingly, however, the distribution in the azimuthal subspace in Fig. 3(l) is essentially not affected by the transformation to *V*-space and remains close to experiment. Overall, the *R*-space structure including quantum as well as thermal fluctuations at 5 K and foil broadening effects is somewhat closer to the experimental data.

Finally, the system was ''heated up'' successively by coupling the molecule to a (Nosé-Hoover-chain [39]) thermal heat bath, see Sec. II. This trick was used in order to excite rovibrational motion, and the notion of ''temperature of the molecule'' should be taken with caution for a system with so few degrees of freedom. At a temperature of the heat bath of 3000 K, the *V*-space distributions as shown in Figs. 3(m)–3(o) were obtained from classical simulations and subsequent foil broadening simulations. Note that at such a high temperature the treatment of the nuclei as classical degrees of freedom is a reasonable approximation. The agreement of the simulated nuclear density distribution function $\rho(E_1, E_2, \phi_{21}, \phi_{13}, S)$ with experiment becomes essentially quantitative at this level of excitation, compare Figs. 3(m)–3(o) to Figs. 3(a)–3(c). A very schematic real-space sketch of the most probable structure that goes with this CEI *V*-space pattern is depicted in Fig. 1(c); again we stress that this is a

very schematic picture of the real situation. The two ''axial protons'' are clearly bent off axis with respect to the C—C bond. In addition, these two protons and the C—C axis are not coplanar, and taking into account the third ''bridging proton,'' a *trans*-bend arrangement occurs. In terms of a dynamical picture that would be consistent with this time-averaged density distribution function, the bridging proton is essentially free to move around the C—C axis. This motion is coupled to a precession motion of the two axial protons around the C—C axis, which is correlated with the orbiting of the axial proton. In summary, the most striking differences of this structure with respect to the bridged equilibrium structure as depicted in Fig. 1(a) is that (i) the $H^{(2)}—C^{(1)}—C^{(2)}—H^{(3)}$ backbone is not even close to being collinear and (ii) that the molecule has a pronounced nonplanarity due to fluctuations, i.e., large-amplitude motion and fluxionality.

IV. CONCLUSIONS AND OUTLOOK

The most probable structure of protonated acetylene $C_2H_3^+$ was investigated in the space spanned by its five internal angular coordinates. The static equilibrium structure of the molecule is well known from reliable electronic structure calculations and can be described as an essentially collinear H—C—C—H backbone with a bridging proton attached to the C—C bond such that *all atoms* share a common plane. Previous data from CEI experiments were reanalyzed in terms of the corresponding nuclear many-body density. They are compared in detail to various *ab initio* simulations with additional inclusion of foil effects that occur during the CEI process, i.e., the *R*-space to *V*-space transformation. It is shown that a classical treatment of the nuclear motion at low temperatures is clearly not appropriate. Upon including nuclear quantum effects such as zero-point motion and tunneling in addition to thermal fluctuations at 5 K, it is found that the most probable ground-state structure of this molecule is nonplanar with a *trans*-bending arrangement of the two ''axial protons.'' Although this is *qualitatively* in accord with the most probable structure inferred from CEI, the experimental structure is far more distorted with respect to the equilibrium structure. However, it can already be concluded at this stage that theoretical approaches that confine all nuclei to move in a common plane are bound to fail in describing this fluxional molecular ion and its large-amplitude motion at a quantitative level. Furthermore, it is observed that *quantitative* agreement with the experimental data is obtained once the molecule is rovibrationally excited.

In conclusion, it seems that $C_2H_3^+$ is flexible enough so that its most probable structure deviates *qualitatively* from its equilibrium structure even at fairly low temperatures where thermal flucuations are negligible. Thus, in order to understand this molecule, the calculation of the nuclear wave function or density matrix is necessary in addition to only locating the global minimum of the potential-energy surface, i.e., the equilibrium structure.

Independent from this assessment, it remains puzzling that only fairly strong excitations lead to a full agreement of the computed and measured nuclear many-body density. Is this an artifact of the CEI process, or is it due to approximations that underly the theoretical treatment? In order to settle this question satisfactorily, significant advances in both experiment and theory are required. Concerning the experiment, it would be highly desirable to be able to control the level of thermal excitations. Such experiments are, in principle, possible using the CEI facility at the heavy-atom storage ring TSR (Testspeicherring) of the MPI Heidelberg, where thermalization down to about 300 K can be achieved [48,49]. Once such experimental data are available, *ab initio* path-integral simulations should be performed at 300 K using a denser discretization of the path integral. In addition, the sampling statistics should be improved in order to capture the dramatic fluctuations that drive the system far away from its equilibrium structure. Thus, $C_2H_3^+$ remains a challenge for the future.

ACKNOWLEDGMENTS

It is a pleasure to thank Dirk Schwalm for his interest and for the support of this study. We gratefully acknowledge invaluable help of Harald Forbert concerning the graphical presentation of the data and we thank FCI for partial financial support.

[1] J.H. Callomon, E. Hirota, T. Iijima, K. Kuchitsu, and W.J. Lafferty, in *Numerical Data and Functional Relationships in Science and Technology*, edited by K.-H. Hellwege and A.M. Hellwege, Landolt-Börnstein, New Series, Group II, Vol. 15 (Springer-Verlag, Berlin, 1987), p. 1; see in particular Table 1.3.3.

[2] *Accurate Molecular Structures—Their Determination and Importance*, edited by A. Domenicano and I. Hargittai (IUCr/ Oxford University Press, Oxford, 1992).

[3] R.D. Brown, in *Structure and Conformations of Non-Rigid Molecules*, edited by J. Laane, M. Dakkouri, B. van der Veken, and H. Oberhammer (Kluwer, Dordrecht, 1993), p. 99.

[4] Z. Vager, R. Naaman, and E.P. Kanter, Science **244**, 426 (1989).

[5] Z. Vager, Adv. At., Mol., Opt. Phys. **45**, 203 (2001).

[6] D. Zajfman, G. Both, E.P. Kanter, and Z. Vager, Phys. Rev. A **41**, 2482 (1990).

[7] D. Zajfman, Phys. Rev. A **42**, 5374 (1990).

[8] D. Zajfman, T. Graber, E.P. Kanter, and Z. Vager, Phys. Rev. A **46**, 194 (1992).

[9] J. Levin, D. Kella, and Z. Vager, Phys. Rev. A **53**, 1469 (1996).

[10] L. Knoll, Direkte Abbildung und Berechnung räumlicher Molekülstrukturen; thesis, Fakultat für Physik und Astronomie, Ruprecht Karls-Universität, Heidelberg, 1997.

[11] R.J. Saykally, Science **239**, 157 (1988).

[12] *Structure and Conformations of Non-Rigid Molecules*, edited by J. Laane, M. Dakkouri, B. van der Veken, and H. Oberhammer (Kluwer, Dordrecht, 1993).

[13] A.E. Glassgold, A. Omont, and M. Guélin, Astrophys. J. **396**, 115 (1992).
[14] B. Zurawski, R. Ahlrichs, and W. Kutzelnigg, Chem. Phys. Lett. **21**, 309 (1973).
[15] T.J. Lee and H.F. Schaeffer III, J. Chem. Phys. **85**, 3437 (1986).
[16] J.A. Pople, Chem. Phys. Lett. **137**, 10 (1987).
[17] R. Lindh, B.O. Roos, and W.P. Kraemer, Chem. Phys. Lett. **139**, 407 (1987).
[18] L.A. Curtiss and J.A. Pople, J. Chem. Phys. **88**, 7405 (1988).
[19] W. Klopper and W. Kutzelnigg, J. Phys. Chem. **94**, 5625 (1990).
[20] C. Liang, T.P. Hamilton, and H.F. Schaefer III, J. Chem. Phys. **92**, 3653 (1990).
[21] R. Lindh, J.E. Rice, and T.J. Lee, J. Chem. Phys. **94**, 8008 (1991).
[22] K. Lammertsma and T. Ohwada, J. Am. Chem. Soc. **118**, 7247 (1996).
[23] J.T. Hougen, J. Mol. Spectrosc. **123**, 197 (1987).
[24] R. Escribano and P.R. Bunker, J. Mol. Spectrosc. **122**, 325 (1987).
[25] R. Escribano, P.R. Bunker, and P.C. Gomez, Chem. Phys. Lett. **150**, 60 (1988).
[26] P.C. Gomez and P.R. Bunker, Chem. Phys. Lett. **165**, 351 (1990).
[27] M. Cordonnier and L.H. Coudert, J. Mol. Spectrosc. **178**, 59 (1996).
[28] J.S. Tse, D.D. Klug, and K. Laasonen, Phys. Rev. Lett. **74**, 876 (1995).
[29] D. Marx and M. Parrinello, Science **271**, 179 (1996).
[30] V.V. Nefedova, A.I. Boldyrev, and J. Simons, J. Chem. Phys. **98**, 8801 (1993).
[31] T. Oka, Philos. Trans. R. Soc. London, Ser. A **324**, 81 (1988).
[32] M.W. Crofton, M.-F. Jagod, B.D. Rehfuss, and T. Oka, J. Chem. Phys. **91**, 5139 (1989).
[33] C.M. Gabrys, D. Uy, M.-F. Jagod, T. Oka, and T. Amano, J. Phys. Chem. **99**, 15 611 (1995).
[34] M. Bogey, M. Cordonnier, C. Demuynck, and J.L. Destombes, Astrophys. J. Lett. **399**, L103 (1992).
[35] M. Bogey, H. Bolvin, M. Cordonnier, C. Demuynck, J.L. Destombes, R. Escribano, and P.C. Gomez, Can. J. Phys. **72**, 967 (1994).
[36] C. Demuynck, J. Mol. Spectrosc. **168**, 215 (1994).
[37] Z. Vager, D. Zajfman, T. Graber, and E.P. Kanter, Phys. Rev. Lett. **71**, 4319 (1993).
[38] E.P. Kanter, Z. Vager, G. Both, and D. Zajfman, J. Chem. Phys. **85**, 7487 (1986).
[39] D. Marx and J. Hutter, in *Modern Methods and Algorithms of Quantum Chemistry*, edited by J. Grotendorst (John von Neumann Institute for Computing, Forschungszentrum Jülich, 2000), pp. 301–449; for downloads see www.theochem.ruhr-uni-bochum.de/go/cprev.html
[40] R. Car and M. Parrinello, Phys. Rev. Lett. **55**, 2471 (1985).
[41] D. Marx and M. Parrinello, Z. Phys. B: Condens. Matter **95**, 143 (1994).
[42] D. Marx and M. Parrinello, J. Chem. Phys. **104**, 4077 (1996).
[43] M.E. Tuckerman, D. Marx, M.L. Klein, and M. Parrinello, J. Chem. Phys. **104**, 5579 (1996).
[44] D. Marx, M.E. Tuckerman, and G.J. Martyna, Comput. Phys. Commun. **118**, 166 (1999).
[45] J. Hutter, P. Ballone, M. Bernasconi, P. Focher, E. Fois, St. Goedecker, D. Marx, M. Parrinello, and M. Tuckerman, CPMD, Version 3.0 (MPI für Festkörperforschung Stuttgart, IBM Research Zurich, 1995-1998).
[46] L. Knoll and D. Marx, Eur. Phys. J. D **10**, 353 (2000).
[47] D. Zajfman, Z. Vager, R. Naaman, R.E. Mitchell, E.P. Kanter, T. Graber, and A. Belkacem, J. Chem. Phys. **94**, 6377 (1991).
[48] R. Wester, F. Albrecht, M. Grieser, L. Knoll, R. Repnow, D. Schwalm, A. Wolf, A. Baer, J. Levin, Z. Vager, and D. Zajfman, Nucl. Instrum. Methods Phys. Res. A **413**, 379 (1998).
[49] A. Baer, M. Grieser, L. Knoll, J. Levin, R. Repnow, D. Schwalm, Z. Vager, R. Wester, A. Wolf, and D. Zajfman, Phys. Rev. A **59**, 1865 (1999).